Condition and Strategy Analysis for Assembly Based on Attractive Region in Environment

Rui Li and Hong Qiao, *Senior Member, IEEE*

***Abstract*—Automatic assembly with high precision is an essential step in robotic manipulation. It is still a difficult problem due to various complicated requirements, such as less contact force, irregular shapes of the parts, sensing information understanding in complex environment, etc. In the previous work, the concept of attractive region in environment (ARIE) was proposed, which helps to achieve high-precision manipulation with low-precision systems by using the constraints formed by the environment. In this paper, the general relation between the physical space and the configuration space for the robotic assembly system will be analyzed, the strategies of using ARIE to achieve high-precision peg-hole assembly will be provided, and furthermore, practical examples for industrial applications will be given, which further illustrates the usefulness of the concept.**

***Index Terms*—Attractive region in environment (ARIE), flexible assembly, robotic assembly system, sensorless manipulation.**

I. Introduction

HOW TO implement an intelligent robotic assembly system is a key problem in industrial applications. In practical application, this can be a very difficult problem due to various requirements. For example, the contact force between the robot and parts should be as small as possible to prevent damages to the parts, the shape of parts to be assembled may be irregular, and therefore, the process of assembly must be investigated and designed, and there are also cases where high-precision sensing is not available during the assembly process.

For years, researchers have studied the modeling of the peg and hole, analyzed the contact states during insertion, and investigated the strategies for specified assembly parts [1], [2]. In recent years, researchers have made great efforts in analyzing manual manipulations to solve the following problems.

1) Using vision/force/laser sensors, the environment and parts of the system can be modeled with high precision. Then, based on the model and comprehension of the environment, relative decisions can be made to achieve high-precision manipulation.
   It should be noted that in such case, modeling requires high-precision information of the parts, which adds an extra cost to the system (this procedure can be seen as "information → decisions").
2) By using the flexibility of hand and the constraints formed by the environment and parts, the uncertainty of the system can be reduced, and then high-precision manipulation can be achieved with a low-precision system (this procedure can be seen as "constraint → decisions") [3], [4].

Various sensor-based approaches have been widely used in robotic assembly applications. Force/torque sensing information has been commonly applied in the robotic assembly system to eliminate the small error in the pose of the parts. Shirinzadeh *et al.* synthesized force/moment information to identify the contact states of a cylindrical pair and developed strategies for minimum-contact-force insertion [5]. Kim *et al.* proposed a shape recognition algorithm and a hole detection algorithm based on a six-axis force/torque sensor system [6]. Jakovljevic *et al.* presented a methodology for generating a fuzzy inference mechanism, which analyzed the force sensing information to determine the contact state of the peg and hole [7].

Image information has also helped in peg-hole assembly. Huang *et al.* realized the dynamic compensation in high-speed assembly through high-speed cameras [8]–[10]. Chang *et al.* installed and tested a high-precision automatic visual-servo microassembly system, which was implemented for micropeg alignment, micropeg transportation, and peg-in-hole assembly [11].

Recently, three-dimensional (3-D) sensing technologies, such as laser, photoelectric, red, green, blue-depth (RGB-D), and multiview stereo vision sensors, have been investigated in the robotic assembly systems [12], [13]. However, sensor-based approaches usually require high-precision sensors to improve the precision of the system, which results in the increase of cost.

Manuscript received September 24, 2016; revised March 26, 2017; accepted May 9, 2017. Date of publication May 16, 2017; date of current version October 13, 2017. Recommended by Technical Editor H. Werner. This work was supported in part by the National Natural Science Foundation of China under Grant 61210009 and Grant 61627808, in part by the Strategic Priority Research Program of the Chinese Academy of Sciences under Grant XDB02080003, and in part by the Beijing Municipal Science and Technology under Grant D16110400140000 and Grant D161100001416001, and in part by the Development of Science and Technology of Guangdong Province Special Fund Project Grants 2016B090910001. *(Corresponding author: Hong Qiao.)*

R. Li is with the State Key Lab of Management and Control for Complex Systems, Institute of Automation, Chinese Academy of Sciences, Beijing 100190, China, and also with the University of Chinese Academy of Sciences, Beijing 100049, China (e-mail: lirui2013@ia.ac.cn).

H. Qiao is with the State Key Lab of Management and Control for Complex Systems, Institute of Automation, Chinese Academy of Sciences, Beijing 100190, China, also with the University of Chinese Academy of Sciences, Beijing 100049, China, and also with the Chinese Academy of Sciences Center for Excellence in Brain Science and Intelligence Technology, Shanghai 200081, China (e-mail: hong.qiao@ia.ac.cn).

Color versions of one or more of the figures in this paper are available online at http://ieeexplore.ieee.org.

Digital Object Identifier 10.1109/TMECH.2017.2705180

In addition, some information cannot be acquired directly from existing sensors.

From another aspect, sensorless approaches have also been investigated for years. Remote center compliance (RCC) and flexible wrist incorporate compliant motion for error correction during assembly. In these years, different kinds of RCC devices have been developed and equipped in robotic assembly tasks. Simunovic [14] and Whitney and Rourke [15] analyzed the utilization and design principles of the flexible wrists. Jain *et al.* demonstrated ionic polymer metal composite (IPMC) fingers based microgripper, in which compliance was added to the system to help achieve micropeg-in-hole assembly [16], [17]. The RCC devices are low cost and reliable for the peg-in-hole assembly. However, the RCC-based method has some problems as follows.

1) It is no longer effective or useful when the contact status of the peg and hole is complex.
2) The materials of the assembly parts are limited.

Recently, vibration has been introduced to help eliminate the deviation in assembly system. Baksys *et al.* discussed the possibility of introducing vibration into the process of passive compliance to help achieve assembly task [18]. Kilikevicius and Baksys found that the vibratory excitation allowed preventing the balance between the insertion force and frictional force to avoid jamming and wedging [19]. Sadauskas *et al.* further analyzed the method for alignment of the parts using high frequency vibrations [20], [21]. However, it remains a problem on how to set proper dynamic system parameters to make alignment process stable and reliable.

For the control of the part-mating process, there have been many related works. Impedance control and force/position control are often considered in such systems. Natale designed a force controller for industrial robot to achieve part-mating tasks. A systematic design procedure to compute structures and parameters of the controller was devised [22]. The main limitation of this method is the performance of the industrial robot applied in the robotic system. Chen *et al.* developed soft servo strategy for a high-precision assembly automation system [23]. Compared with force control methods, the contact forces can be controlled directly and greater part location errors can be eliminated. However, the proposed method may result in failure since it could generate larger contact forces than allowed. Kwak *et al.* studied the method to elimination of unnecessary contact state for robotic assembly tasks [24]. They used graph to describe the contact state and discovery unnecessary contact state. Takahashi proposed a passive alignment principle for very high precision robotic assembly. In this method, they used compliance control in directions of two axes to enable compliance to perform the mating action while keeping contact force between the assembly parts [25]. The method made it possible to achieve the assembly task with a robot whose precision does not meet the task requirement. But the shape of the assembly parts cannot be generalized.

In the previous work, the mathematical definition of attractive region in environment (ARIE) was discussed, and the condition of the existence of ARIE in different configuration space was analyzed [26]. A vision-based peg-hole insertion system with specialized pushing device was designed [27]. In this paper, the conditions and strategies of using ARIE to achieve flexible and reliable assembly operation will be given, and an industrial robot-based peg-hole insertion strategy will be implemented.

TABLE I
DEFINITION OF NOTIONS

Symbol	Definition
$O_h X_h Y_h Z_h$	Coordinate frame fixed to the hole, where O_h is defined as the center of the upper surface of the hole, $O_h Y_h$ is defined as the line from O_h along the wrist of the robot to the base of the robot, $O_h Z_h$ is along the axis of the hole upwards and $O_h X_h$ is perpendicular to $O_h Y_h$ and $O_h Z_h$ and satisfies the right hand rule.
S_{solid}	The solid part around the hole as shown in Fig. 1.
S_{hole}	The hole as shown in Fig. 1.
S_{peg}	The peg as shown in Fig. 1.
O_p	The center of the end surface of the peg.
L_p	The lowest point on the peg along $O_h Z_h$ -axis in $O_h X_h Y_h Z_h$ frame.
C_{free}	The free configuration space of the peg.
Ω_{peg}	The constrained region of the peg in configuration space.
$\left[\bullet\right]$	The boundary of $\bullet$.
$\left(\bullet\right)$	The inner part of $\bullet$ (The boundary is not included).
CP_{peg}	The set of contact points of the peg and hole on the peg.
CP_{hole}	The set of contact points of the peg and hole on the hole.
$\text{traj}(p)$	The enclosed trajectory formed by a certain point p.

The rest of this paper is arranged as follows. In Section II, the formation of ARIE in assembly systems will be illustrated. In Section III, the relation between the shape of constrained region in configuration space and that of the peg and hole in physical space will be analyzed. In Section IV, several assembly strategies will be given through the analysis of the ARIE formed for different assembly parts. In Section V, a detailed application of the ARIE in two types of peg-hole assembly of rot-vector (RV) reducer for industrial manufacturing will be given.

II. ARIE FORMED IN PEG-HOLE ASSEMBLY TASKS

In this section, some coordinate frame and symbols will be introduced to illustrate the formation of ARIE in peg-hole assembly tasks. Some notations are defined in Table I.

As shown in Fig. 1, a coordinate frame $O_h X_h Y_h Z_h$ is fixed on the hole. Base point O_h of the coordinate is defined as the center of the upper surface of the hole, axis $O_h Z_h$ is along the axis of the hole upwards, and axes $O_h X_h$ and $O_h Y_h$ are orthogonal in the upper surface of the hole. The axes $O_h X_h$, $O_h Y_h$, and $O_h Z_h$ satisfy the right-hand rule with them. Similarly, a coordinate frame $O_p X_p Y_p Z_p$ is attached to the peg. Base point O_p of the coordinate is defined as the center of the lower surface of the peg, axis $O_p Z_p$ is along the axis of the peg upwards, and axes $O_p X_p$ and $O_p Y_p$ are orthogonal in the upper surface of the hole. Then, the configuration of the peg in the $O_h X_h Y_h Z_h$-frame can be described as $P_{\text{peg}} = (p_{\text{ph}}, R_{\text{ph}}) = [|O_h O_p|_{X_h}, |O_h O_p|_{Y_h}, |O_h O_p|_{Z_h}, \theta_{X_h}, \theta_{Y_h}, \theta_{Z_h}]^T$, where $p_{\text{ph}} = [|O_h O_p|_{X_h}, |O_h O_p|_{Y_h}, |O_h O_p|_{Z_h}]^T \in \mathbb{R}^3$ is the position vector of the peg and $R_{\text{ph}} \in SO(3)$ is the orientation of the peg frame relative to the hole frame, which can be parameterized as RPY angles $\theta_{\text{ph}} = [\theta_{X_h}, \theta_{Y_h}, \theta_{Z_h}]^T = [\langle \overrightarrow{O_p Z_p}, \overrightarrow{O_h X_h} \rangle, \langle \overrightarrow{O_p Z_p}, \overrightarrow{O_h Y_h} \rangle, \langle \overrightarrow{O_p Z_p}, \overrightarrow{O_h Z_h} \rangle]^T$.

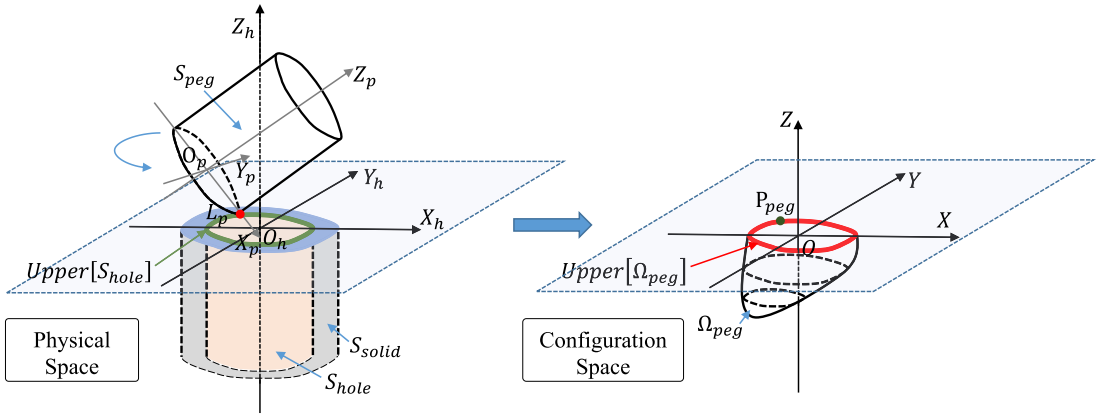

Fig. 1. *Left*: $O_h X_h Y_h Z_h$ Coordinate frame established for the peg-hole system. *Right*: Constrained region formed by the round-peg and round-hole in configuration space when the rotational angles of the peg are fixed. According to Definition 1, the constrained region is an ARIE.

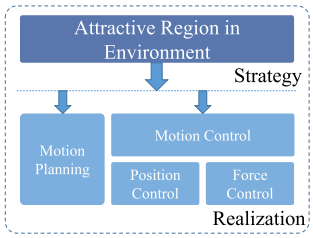

Fig. 2. Structure of an ARIE-based robotic manipulation system.

In the peg-hole assembly process, the environment constraints C_{env} is the set of all of the contact states of the peg and hole: $C_{\text{env}} = \{P_{\text{peg}} \in SE(3) \mid [S_{\text{peg}}] \cap [S_{\text{solid}}] \neq \phi, (S_{\text{peg}}) \cap (S_{\text{solid}}) = \phi\}$, where $[\bullet]$ means the boundary of $\bullet$, and $(\bullet)$ means the inner part of $\bullet$, as described in Table I. It is noted that C_{env} describes the geometry of the boundary of the free configuration space of the peg. According to the definition in [26], if there exist a region Ω in the free configuration space of the peg, the boundary of which is formed by the environment constraints, and a state-independent input can be found under which the state will converge to a stable point, then the region Ω is an ARIE.

For an intuitive understanding, Fig. 1 displays an ARIE in $\mathbb{R}^3$ formed by round peg and round hole given a fixed orientation of the peg. It can be seen that ARIE constructs the relation between the environment constraint with the state of the system, which makes it possible to design manipulation strategies for robotic systems.

The structure of an ARIE-based robotic manipulation system is depicted in Fig. 2. On the top level, the existence of ARIE in the targeted system should be investigated. If so, strategies could be designed based on the geometry of the environment constraints. Correspondingly, the motion planning and control can be determined according to the strategy.

III. Relation Between ARIE in Configuration Space and Assembly Parts in Physical Space

In this section, the theoretical analysis on the relation between the shape of constrained region in configuration space and that of assembly parts in physical space will be given. For convenience, peg-hole insertion is taken as an example of assembly tasks. The relation between the physical space and the configuration space, the shape of the hole and that of the constrained region, and the shape of the peg and that of the constrained region will be separately discussed.

A. Relation Between the Physical Space and the Configuration Space

For clearance and better understanding, the coordinate frames used in the peg-hole system will be introduced. As stated in Section II, $O_h X_h Y_h Z_h$ frame is attached to the hole and $O_p X_p Y_p Z_p$ frame is attached to the peg, respectively. The configuration of the peg can be described in $O_h X_h Y_h Z_h$ frame as $P_{\text{peg}} = [|O_h O_p|_{X_h}, |O_h O_p|_{Y_h}, |O_h O_p|_{Z_h}, \theta_{X_h}, \theta_{Y_h}, \theta_{Z_h}]^T \triangleq [x, y, z, \theta_{X_h}, \theta_{Y_h}, \theta_{Z_h}]^T \in C_{\text{env}} \subset SE(3)$.

The free configuration space C_{free} of the peg is defined as the set of configurations of the peg that satisfy the rigid constraint

$$C_{\text{free}} = \left\{ P_{\text{peg}} \in SE(3) \,\middle|\, \left(S_{\text{peg}}\right) \cap \left(S_{\text{solid}}\right) = \phi \right\}. \quad (1)$$

The constrained region of the peg formed by the hole is

$$\Omega_{\text{peg}} = \{P_{\text{peg}} \in C_{\text{free}} \,|\, S_{\text{peg}} \cap S_{\text{hole}} \neq \phi\}. \quad (2)$$

Fig. 1 gives an intuitive illustration of notions defined above. It can be seen that S_{peg}, S_{solid}, and S_{hole} are defined in the physical space, which represent the objects; P_{peg} and Ω_{peg} are defined in the configuration space, which represent regions formed by different constraints.

B. Relation Between Geometry of Hole and Constrained Region

Lemma 1: If there exists a contact point between the peg and hole in the physical space, then the corresponding configurations of the peg are on the boundary of the constrained region of the peg in the configuration space.

Proof: Suppose cp is a contact point between the peg and hole in the physical space. That is, $cp \in CP_{\text{peg}} \cap CP_{\text{hole}}$, then $cp \in [S_{\text{peg}}] \cap [S_{\text{hole}}] \subset S_{\text{peg}} \cap S_{\text{hole}}$.

Let the configuration of the peg be P_{peg}, which corresponds to cp. Then, according to the definition of Ω_{peg}, it follows that $P_{\text{peg}} \in \Omega_{\text{peg}}$.

On the other hand, since $cp \in [S_{\text{hole}}]$, for any $\epsilon > 0$, there is a $cp^1 \in (S_{\text{solid}})$(which means $cp^1 \notin S_{\text{hole}}$) such that the distance between cp and cp^1 is ϵ. That is, cp can be moved to cp^1 in a distance ϵ away from the hole. Since the configuration of the peg P_{peg} is continuous with respect to the movement of cp, the configuration P^1_{peg} of the peg corresponding to cp^1 is not in Ω_{peg} (this is because $cp^1 \in S_{\text{peg}}$ but $cp^1 \notin S_{\text{hole}}$). That is, $P^1_{\text{peg}} \notin \Omega_{\text{peg}}$.

Therefore, $P_{\text{peg}} \in [\Omega_{\text{peg}}]$, which is the boundary of Ω_{peg}.

Theorem 1: For the peg of which the orientation R_{ph} is fixed, the shape of the upper surface of the constrained region is that of the upper surface of the hole if the lowest point L_p of the peg is a unique point.

Proof: As proven in Lemma 1, if the peg touches the hole, then the configuration of the peg satisfies $P_{\text{peg}} \in [\Omega_{\text{peg}}]$.

It can be concluded that $P_{\text{peg}} \in \Omega_{\text{peg}}$, and $S_{\text{peg}} \cap S_{\text{hole}} \neq \phi$. If the orientation R_{ph} of the peg is fixed, the configuration of the peg P_{peg} can be represented in $\mathbb{R}^3$ configuration space with respect to $[x, y, z]^T$, as illustrated in Fig. 1.

It can be seen that the mouth (upper surface) of $[\Omega_{\text{peg}}]$ is made up of the configurations P^*_{peg} of the peg of which the z-component is the maximum in Ω_{peg}. In such case, $P^*_{\text{peg}} \in \Omega_{\text{peg}}$, and $S_{\text{peg}} \cap S_{\text{hole}} \neq \phi$. Therefore, there exists at least one contact point between the peg and the hole. Let the contact point(s) be CP_{peg}, CP_{hole}. Since the z-component of the peg is maximum, the contact point(s) on the peg CP_{peg} has to be within the lowest point(s) of the peg L_p, and the contact point(s) on the hole CP_{hole} has to be within the upper surface of the hole, that is, $CP_{\text{peg}} \subseteq L_p$, and $CP_{\text{hole}} \subseteq \text{Upper}[S_{\text{hole}}]$. Given the above equations, it can be concluded that $CP_{\text{peg}} = L_p$.

Suppose that the lowest point of the peg L_p is a unique point, then $CP_{\text{peg}} = L_p = p$; $\therefore$ CP_{hole} can be any point in $\text{Upper}[S_{\text{hole}}]$.

Furthermore, if the lowest point of the peg touches the mouth of the hole, which means $L_p \in \text{Upper}[S_{\text{hole}}]$, then it can be concluded that $P^*_{\text{peg}} \in \text{Upper}[\Omega_{\text{peg}}]$, and the shape of the mouth of $[\Omega_{\text{peg}}]$ is the shape of the trajectory of L_p [that is, traj(L_p)], and

$$L_p \in \text{Upper}\left[S_{\text{hole}}\right] \rightarrow \text{traj}\left(L_p\right) = \text{Upper}\left[S_{\text{hole}}\right].$$

Finally, it can be concluded that the shape of $\text{Upper}[\Omega_{\text{peg}}]$ is the same as that of $\text{Upper}[S_{\text{hole}}]$. ■

This theorem can be intuitively illustrated as Fig. 1. If the lowest point of the peg L_p is a unique point, then the shape of the mouth (upper surface) of the constrained region is the trajectory of L_p, which moves along the mouth of the hole. Therefore, the shape of the mouth of the constrained region is exactly the same as that of the mouth of the hole.

Remark 1: Theorem 1 reveals the relation between the shape of the mouth of constrained region and that of the hole. This theorem explains why force sensor may not work effectively in cases where the lowest point L_p touches the mouth of the hole. No matter where the peg is, the force/torque information collected by the sensor will not change since the contact relation does not change.

C. Relation Between Geometry of Peg and Constrained Region

In Section III-B, the relation between the shape of the hole and the constrained region has been explained. In this part, the relation between the shape of the peg and the constrained region will be discussed. Three different cases, i.e., round-peg-round-hole insertion, convex-polygon-peg-round-hole insertion, and convex-polygon-peg-convex-polygon-hole insertion will be considered.

For the configuration of the peg $P_{\text{peg}} = [x, y, z, \theta_{X_h}, \theta_{Y_h}, \theta_{Z_h}]^T$, if the rotational angles are fixed, the configuration of the peg can be represented in $\mathbb{R}^3$ configuration space with respect to $[x, y, z]^T$. Suppose z is given satisfying $P_{\text{peg}} \in \Omega_{\text{peg}}$, then the configuration of the peg will form a constrained region in $\mathbb{R}^2$ configuration space, the boundary of which is made up of the trajectories of the contact points of the peg and hole, according to Lemma 1.

Theorem 2: For round-peg-round-hole insertion, if the orientation R_{ph} of the peg is fixed and the translational position z is given, then the shape of the cross sections of the constrained region parallel to $X_hO_hY_h$ plane is made up of three parts: two arcs, which are part of the mouth of the hole, and a curve, which is relevant to both the hole and peg.

Proof: If the peg touches the hole, the configuration of the peg satisfies $P_{\text{peg}} \in [\Omega_{\text{peg}}]$. It can be concluded that $P_{\text{peg}} \in \Omega_{\text{peg}}$, $CP_{\text{peg}} = S_{\text{peg}} \cap S_{\text{hole}} \neq \phi$, $CP_{\text{hole}} = S_{\text{peg}} \cap S_{\text{hole}} \neq \phi$. According to the constraint of rigid body, the contact point(s) on the hole satisfies $CP_{\text{hole}} \subseteq [S_{\text{hole}}]$ or $CP_{\text{hole}} \subseteq \text{Upper}[S_{\text{hole}}]$. For high-precision peg-hole insertion, the clearance between the parts is very small. If the fixed orientation R_{ph} is not zero, then only $CP_{\text{hole}} \subseteq \text{Upper}[S_{\text{hole}}]$ holds (see [1]).

Suppose the z-component of the peg is given, the contact point(s) on the peg satisfies $CP_{\text{peg}} \subseteq [\text{Proj}(S^z_{\text{peg}})]$, where $(\text{Upper}[S_{\text{hole}}]) \cap S_{\text{peg}} \triangleq \text{Proj}(S^z_{\text{peg}})$, in which $(\text{Upper}[S_{\text{hole}}])$ means the inner part of the mouth of the hole in $X_hO_hY_h$ plane [as shown in Fig. 3(a)], and $\text{Proj}(S^z_{\text{peg}})$ means the cross section of the peg cut by $(\text{Upper}[S_{\text{hole}}])$, given the z-component of the peg.

It can be proven that $\text{Proj}(S^z_{\text{peg}})$ is made up of a line segment (when the end surface of the peg is a plane) and an elliptical arc. According to Lemma 1, it is known that the boundary of the cross section of the constrained region parallel to $X_hO_hY_h$ plane is the set of configurations that the peg touches the hole. That is, $[\text{Proj}(S^z_{\text{peg}})] \cap \text{Upper}[S_{\text{hole}}] \neq \phi$.

To analyze the shape of the boundary of the cross section of the constrained region, the contact points should be found first. The shape of the boundary of the cross section of the constrained region can be given as

$$\text{traj}\left(\text{Proj}\left(S^z_{\text{peg}}\right)\right) = \bigcup_i \text{traj}\left(CP^i\right).$$

There are two cases of the position of the contact points that should be considered, respectively.

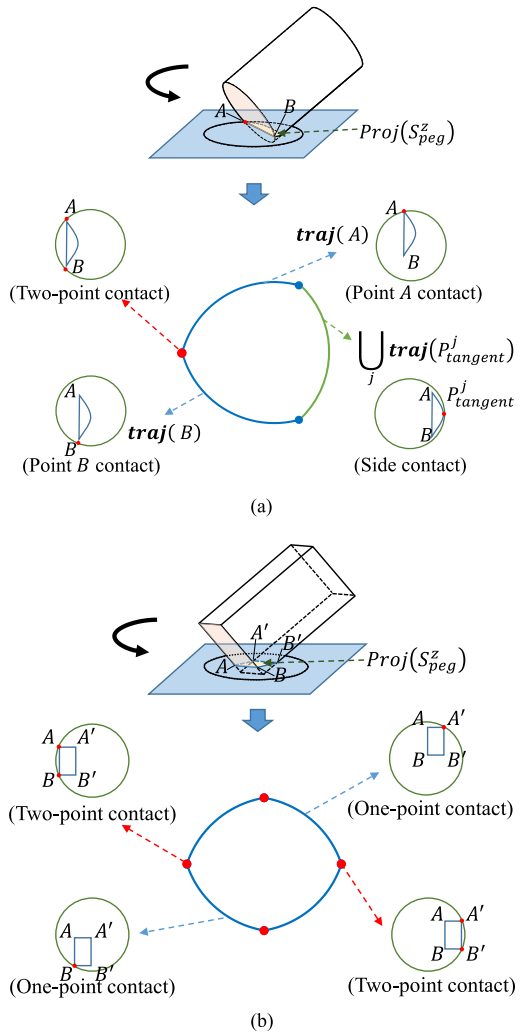

Fig. 3. Shape of the cross section of the constrained region parallel to $X_hO_hY_h$ plane is the shape of the trajectory of $\mathrm{Proj}(S^z_{\mathrm{peg}})$ for (a) round-peg-round-hole insertion and (b) convex-polygon-peg-round-hole insertion (the cuboid is taken as an example).

Case 1: If the line segment touches the hole, the contact point is the end point.

Proof: Let the line segment be $\overline{AB}$, and assume that there is a contact point $P \in \overline{AB}$ and $P \neq A, P \neq B$. Then, $\overline{AB}$ may be 1) tangent to, or 2) intersecting to the mouth of the hole. If 1) holds, then P is the tangent point and $A \notin S_{\mathrm{hole}}, B \notin S_{\mathrm{hole}}$, where the rigid constraint is not satisfied; and if 2) holds, then P is the intersecting point and $A \notin S_{\mathrm{hole}}, B \in S_{\mathrm{hole}}$(or $A \in S_{\mathrm{hole}}, B \notin S_{\mathrm{hole}}$), where the rigid constraint is not satisfied, either.

Therefore, if the line segment touches the hole, the contact point has to be the end point of the segment.

Case 2: If the elliptical arc touches the hole, the contact point is the tangent point.

Proof: This holds for the reason that if the elliptical arc and the mouth of the hole intersects, then the end points of elliptical arc have to be on the different sides of the hole. Note that "the elliptical arc is tangent to the mouth of the hole in an arbitrary point P" means that, the gradient of the elliptical arc on P is the same with that of the mouth of the hole on P.

Given *Case 1* and *Case 2* above, the shape of the boundary of the cross section of the constrained region can be formulated as

$$\begin{aligned}\mathrm{traj}\left(\mathrm{Proj}\left(S^z_{\mathrm{peg}}\right)\right) &= \mathrm{traj}\left(A\right)\\ &\cup \mathrm{traj}\left(B\right)\\ &\cup \bigcup_j \mathrm{traj}\left(P^j_{\mathrm{tangent}}\right),\end{aligned}$$

where A, B are the end points of the line segment, and P^j_{tangent} is the jth tangent point of the elliptical arc and the mouth of the hole. This can be illustrated in Fig. 3(a).

Theorem 3: For convex-polygon-peg-round-hole insertion, if the orientation R_{ph} of the peg is fixed and the translational position z is given, then the shape of the cross sections of the constrained region parallel to $X_hO_hY_h$ plane is made up of n arcs, which are part of the mouth of the hole, where n is the number of vertexes of the cross section of the peg.

Proof: The proof of this theorem is the same as above except that the cross section of the peg $\mathrm{Proj}(S^z_{\mathrm{peg}})$ is a convex polygon, and only *Case 1* of Theorem 2 holds. Therefore, the contact point(s) CP_{peg} are all vertexes of $\mathrm{Proj}(S^z_{\mathrm{peg}})$. According to Theorem 2, the trajectory of $\mathrm{Proj}(S^z_{\mathrm{peg}})$ is

$$\begin{aligned}\mathrm{traj}\left(\mathrm{Proj}\left(S^z_{\mathrm{peg}}\right)\right) &= \bigcup_i \mathrm{traj}\left(CP^i\right)\\ &= \bigcup_{i=1}^{n} \mathrm{traj}\left(P^i_{\mathrm{vertex}}\right)\end{aligned}$$

[as shown in Fig. 3(b)] where P^i_{vertex} is the ith vertex point of $\mathrm{Proj}(S^z_{\mathrm{peg}})$. ■

Theorem 4: For convex-polygon-peg-convex-polygon-hole insertion, if the orientation R_{ph} of the peg is fixed and the translational position z is given, then the shape of the cross sections of the constrained region parallel to $X_hO_hY_h$-plane is a convex polygon, of which the sides are all parallel to the sides of the mouth of the hole.

Proof: The proof of this theorem is the same as above except that the shape of the mouth of the hole is a convex polygon, in which case the contact point may be within the line segment, if the line segment is parallel to the side of mouth of the hole. According to Theorem 3, the trajectory of $\mathrm{Proj}(S^z_{\mathrm{peg}})$ is

$$\begin{aligned}\mathrm{traj}\left(\mathrm{Proj}\left(S^z_{\mathrm{peg}}\right)\right) &= \bigcup_i \mathrm{traj}\left(CP^i\right)\\ &= \bigcup_{i=1}^{m} \mathrm{traj}\left(P^i_{\mathrm{vertex}}\right).\end{aligned}$$

Remark 2: Theorems 2–4 analyze the relation between the shape of the peg and that of the cross section of constrained region parallel to $X_hO_hY_h$ plane. In general, the shape of the cross section of constrained region is determined by the shape of the peg and the hole. It is found that when the contact points are the vertexes of the cross section of the peg $\mathrm{Proj}(S^z_{\mathrm{peg}})$, the shape of the cross section of constrained region is still determined by the shape of the mouth of the hole. Furthermore, when the contact point is a fixed point on the peg, the trajectory of this point forms a curve on the boundary of constrained region, which is part of the shape of the hole; on the other hand, when the contact point is a fixed point on the hole, the trajectory of this point forms a curve on the boundary of constrained region, which is part of the shape of the peg.

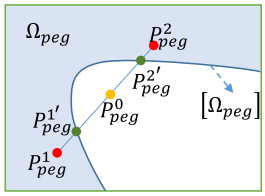

Fig. 4. Illustration of Theorem 5. The curve from $P^{1'}_{\text{peg}}$ to $P^{2'}_{\text{peg}}$ describes either the shape of the peg or that of the hole, which indicates either the peg or the hole is nonconvex.

Theorem 5: For convex-peg-convex-hole insertion, if the orientation R_{ph} of the peg is fixed, then there exists an ARIE in the $\mathbb{R}^3$ configuration space of the peg.

Proof: For convex peg S_{peg} and convex hole S_{hole}, that is $S_{\text{peg}} \to \text{convex}$, and $S_{\text{hole}} \to \text{convex}$. If the rotational angles of the peg are fixed, then the configuration of the peg can be represented in $\mathbb{R}^3$ configuration space with respect to $[x, y, z]^T$.

As shown in Fig. 4, suppose that the constrained region of the peg in $\mathbb{R}^3$ configuration space is not convex, that is $\Omega_{\text{peg}} \to \text{nonconvex}$, then there exist $P^1_{\text{peg}} \in \Omega_{\text{peg}}$, $P^2_{\text{peg}} \in \Omega_{\text{peg}}$ and a real number $t_0 \in (0, 1)$ satisfying $P^0_{\text{peg}} = (1 - t_0)P^1_{\text{peg}} + t_0 P^2_{\text{peg}} \notin \Omega_{\text{peg}}$. Since $P^1_{\text{peg}} \in \Omega_{\text{peg}}$, $P^0_{\text{peg}} \notin \Omega_{\text{peg}}$, and Ω_{peg} is continuous, there should exist a point $P^{1'}_{\text{peg}} = (1 - t^{1'})P^1_{\text{peg}} + t^{1'}P^0_{\text{peg}} \in [\Omega_{\text{peg}}]$. Similarly, there should exist a point $P^{2'}_{\text{peg}} = (1 - t^{2'})P^2_{\text{peg}} + t^{2'}P^0_{\text{peg}} \in [\Omega_{\text{peg}}]$.

Therefore, there should exist a curve l from $P^{1'}_{\text{peg}}$ to $P^{2'}_{\text{peg}}$. According to Lemma 1, l is a set of configurations of the peg in which the peg touches the hole. According to Remark 2, l indicates either the peg or the hole is nonconvex, which is inconsistent with the assumed condition that the peg and hole are all convex. Therefore Ω_{peg} should be convex.

Finally, according to [24, Th. 2], since the constrained region Ω_{peg} is convex, it is an ARIE. ■

Remark 3: Theorem 5 interprets the existence of ARIE in assembly systems. If the parts are convex, then there will always exist an ARIE, which can be utilized for strategy investigation for the insertion process.

Remark 4: Theorems 1–5 reveal the geometry relation between constrained region in $\mathbb{R}^3$ configuration space and assembly parts in physical space. For peg-hole assembly tasks, it is possible to determine the direction of a state-independent input u for the configuration of the peg P_{peg}, given the geometry of the boundary of the ARIE, and then P_{peg} will converge to a stable point with the effect of u. Therefore, ARIE bridges the geometry analysis with the dynamics of the assembly system from the perspective of robotic manipulation strategy design.

IV. Strategy Investigation for Peg-Hole Assembly Using the Concept of ARIE

In this section, the strategy of using the ARIE to find a valid assembly process will be presented. Assembly strategies for round-peg-hole insertion and convex-polygon-peg-hole insertion will be discussed separately.

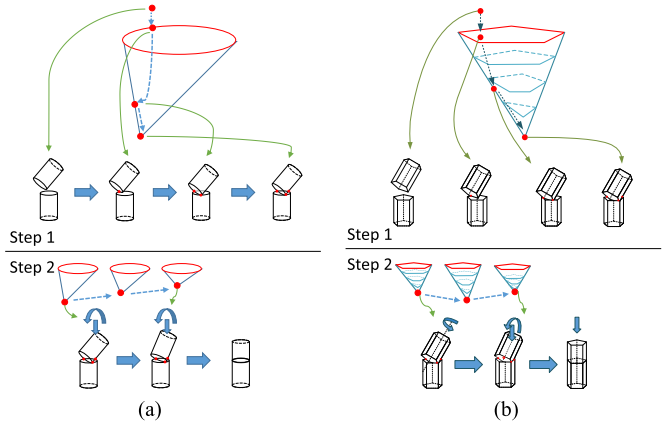

Fig. 5. (a) Two-step insertion strategy for round-peg and round-hole. Step 1: A constant force in vertical direction is applied to push the peg into three-point contact state. Step 2: keep the force applied, and rotate the peg around $O_h X_h$-axis or $O_h Y_h$-axis step by step to finish the insertion. (b) Two-step insertion strategy for convex-polygon-peg and convex-polygon-hole. Step 1: A constant force in vertical direction is applied to push the peg into the strictly stable state. Step 2: Rotate the peg around its rotational axis to eliminate $\Delta\theta_z$ and then keep the force applied, and rotate the peg around the $O_h X_h$-axis or $O_h Y_h$-axis step by step to finish the insertion.

A. Strategy for Round-Peg-Hole Insertion

Because of the rotational symmetry of the round peg, the initial uncertainty of the configuration of the peg is $\Delta P_{\text{peg}} = [\Delta x, \Delta y, \Delta z, \Delta\theta_x, \Delta\theta_y, 0]^T$. A two-step strategy can be designed based on ARIE.

Step 1: Rotate the peg around $O_h X_h$-axis or $O_h Y_h$-axis by θ_r, which guarantees the existence of ARIE with the assumption that $|\theta_{\text{peg}}|_x \gg \Delta\theta_x$, $|\theta_{\text{peg}}|_y \gg \Delta\theta_y$. Keep the orientation R_{ph} of the peg fixed, and then there exists an ARIE in $\mathbb{R}^3$ configuration space $C_{\text{free}}^{R_{\text{ph}}(\theta_{\text{ph}}=\theta_r)}$.

To eliminate the uncertainty of Δx, Δy, and Δz, a constant input u along the negative direction of $O_h Z_h$-axis can be designed in $C_{\text{free}}^{R_{\text{ph}}(\theta_{\text{ph}}=\theta_r)}$. As shown in Fig. 1, if the state of the peg is within the initial range (the upper mouth of the ARIE), then it will converge to the stable point with the effect of u. Since there exists only one strict stable point in the configuration space of round-peg and round-hole system, the uncertainty of Δx, Δy, and Δz is eliminated.

Step 2: Rotate the peg around $O_h X_h$-axis (or $O_h Y_h$-axis) by $-\theta_r$ to eliminate the uncertainty of $\Delta\theta_x$ and $\Delta\theta_y$. During the rotation process, keep the force applied, and rotate the peg around $O_h X_h$-axis or $O_h Y_h$-axis step by step, until $|\boldsymbol{\theta}| = 0$. Then, the peg will be pushed into the hole, and the uncertainty of $\Delta\theta_x$ and $\Delta\theta_y$ is eliminated. The whole procedure is shown in Fig. 5(a).

B. Strategy for Convex-Polygon-Peg-Hole Insertion

When assembling a convex polygon peg into the hole, the initial uncertainty of the configuration of the peg is $\Delta P_{\text{peg}} = [\Delta x, \Delta y, \Delta z, \Delta\theta_x, \Delta\theta_y, \Delta\theta_z]^T$, where $\Delta\theta_z$ means the deviation angle about the rotational axis of the peg. To eliminate $\Delta\theta_z$, the rotational angle of the peg should be considered.

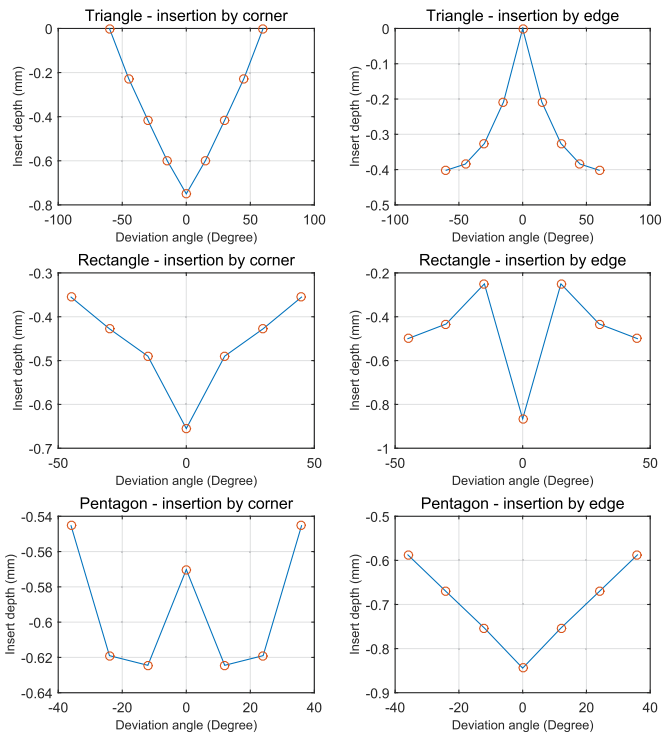

Fig. 6. Relation between deviation angle and insertion depth. This relation changes according to the contact type of the peg and hole, which means whether the peg touches the edge or the corner of the upper surface of the hole. For different shapes of peg and hole, there may exist 2-D ARIE. As shown above, for triangle-peg and triangle-hole, when the peg touches the corner of the upper surface of the hole, there exists a 2-D ARIE.

Step 1: Rotate the peg around O_hX_h-axis or O_hY_h-axis by θ_r, which guarantees the existence of ARIE with the assumption that $|\theta_{\text{peg}}| \gg \Delta\theta_x$, $|\theta_{\text{peg}}| \gg \Delta\theta_y$. Keep the orientation R_{ph} of the peg fixed, and then there exists an ARIE in $\mathbb{R}^3$ configuration space $C_{\text{free}}^{R_{\text{ph}}(\theta_{\text{ph}}=\theta_r)}$.

Step 2: Rotate the peg around its rotational axis to eliminate $\Delta\theta_z$. Finally, keep the force applied, and rotate the peg around O_hX_h-axis or O_hY_h-axis step by step until $|\boldsymbol{\theta}| = 0$. Then, the peg will be pushed into the hole, and the uncertainty of $\Delta\theta_x$ and $\Delta\theta_y$ is eliminated. The whole procedure is shown in Fig. 5(b).

Remark 5: To eliminate $\Delta\theta_z$, the orientation of the hole should also be considered. When rotating the peg around its rotational axis, the insertion depth changes. And the relation between the deviation angle and insertion depth is related to the contact type of the peg and hole, which means whether the peg touches the edge or the corner of the upper surface of the hole. As shown in Fig. 6 , for different shapes of peg and hole, there may exist 2-D ARIE for a certain orientation of the hole, which can be utilized to eliminate $\Delta\theta_z$.

Remark 6: According to the strategies discussed above, it should be noted that there are some perquisite requirement for the robotic manipulator.

1) The manipulator has the ability to keep the orientation of the object fixed while moving.
2) The manipulator has the ability to move along the Z_h-axis in a compliant manner while the position of the object along X_h- and Y_h-axis is not controlled.

Remark 7: In industrial application, chamfer is widely used for assembly tasks, which helps the initial stage of the insertion process. However, chamfer requires additional machining process of the parts, and chamfer cannot lower the requirement for the precision of the robotic system. On the other hand, introducing chamfer to the insertion process can be seen as a method that enlarges the initial range of the ARIE. For example, assume that the radius of the hole is r_{hole} and the radius of the upper surface of the chamfer is r_c ($r_c > r_{\text{hole}}$), then the initial range where the peg can be inserted with the ARIE-based strategy would be enlarged from r_{hole} to r_c.

V. Application: Using ARIE to Achieve Part Assembly for RV Reducer

As proven in Section III, attractive regions in environment widely exist in assembly systems. One application of example is the assembly of RV reducer. RV reducer is a new kind of planetary reducer that has excellent features, e.g., high torque density, high shock load capability, high rigidity, high precision, etc.; therefore, it is widely used in robotic and other high-precision systems.

RV reducer is made up of the following key components: 1) case; 2) shaft and hold flange; 3) eccentric crankshaft; 4) RV gears; and 5) input and spur shafts.

In this paper, the strategy for crankshaft-bearing insertion and the input shaft insertion will be proposed, which is the main difficulty of the whole assembly task. The eccentricity of the crankshaft and the gear part of the input shaft add the complexity of the process. The computer aided design (CAD) models of crankshaft and the input shaft are shown in Fig. 7(a).

During the real experiment, it is noted that the velocity of the end effector should be confined within a certain range V_{safe}, which guarantees a damage-free contact. Since the proposed method is model based, it is easy to determine a "safe distance" ϵ. The velocity of the end effector should be reduced to $v \in V_{\text{safe}}$ before the end effector enters the "safe distance."

In this application, the assembly process will be first analyzed in a simulation environment, and then the strategy will be applied to the laboratory experiments to illustrate the effectiveness of the method. The whole process of the assembly is illustrated in Algorithm 1.

A. Analysis in the Simulation Environment for the Assembly System

In this paper, the assembly process is simulated with MSC.ADAMS. Automated dynamic analysis of mechanical systems (ADAMS) is a multibody dynamics simulation software, which is capable of calculating the pose (position and orientation), motion (velocity and acceleration), contact (contact force and contact points), etc.

In the simulation, the CAD model should be imported first and then the initial conditions should be set for the assembly parts. For simplicity, the parts to be assembled (the eccentric crankshaft and the input shaft) will be set in the state of uniform motion with a proportional controller.

The coordinate frames are defined as follows.

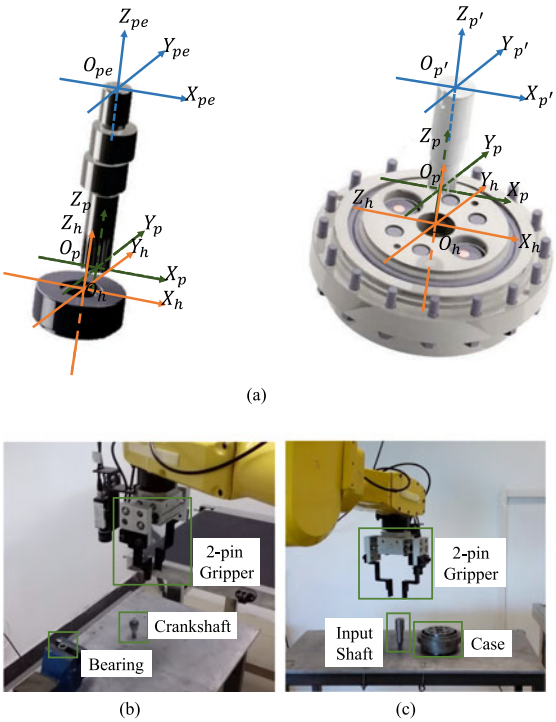

Fig. 7. (a) CAD models for the eccentric crankshaft-bearing insertion and the input shaft insertion. *Left:* The diameter of the lower part of the crankshaft is 9.75 mm, and the inner diameter of the bearing is 9.80 mm. *Right:* The diameter of the input shaft is separately 29.50 mm, 26.50 mm, and 22.50 mm (from top to bottom), and the inner diameter of the upper surface of the flange is 30.00 mm. (b) Experimental setup for crankshaft-bearing assembly. (c) Experiment setup for input shaft case assembly.

Algorithm 1: ARIE-based algorithm for peg-hole insertion.

Require:
Model information S_{peg} and S_{hole}.
Ensure:
Possible assembly strategy.
1: Generate the constrained region of the peg Ω_{peg} and determine the existence of ARIE in $\mathbb{R}^n$, where n is the number of dimension of the configuration space of the peg. Let $\Omega^*_{\text{peg}} = \Omega_{\text{peg}}$;
2: **if** $\Omega^*_{\text{peg}} \rightarrow ARIE$ **then**
3: **repeat**
4: Find/Design a state-independent input $u(t)$.
5: Construct the trajectory of the peg with $u(t)$ applied.
6: **until** $\Delta P_{\text{peg}} = 0$
7: **else**
8: Project Ω_{peg} in $\mathbb{R}^n$ to subspaces $\hat{\Omega}_{\text{peg}}$ and determine the existence of ARIE. Let $\Omega^*_{\text{peg}} = \hat{\Omega}_{\text{peg}}$. Goto Step 2;
9: **end if**

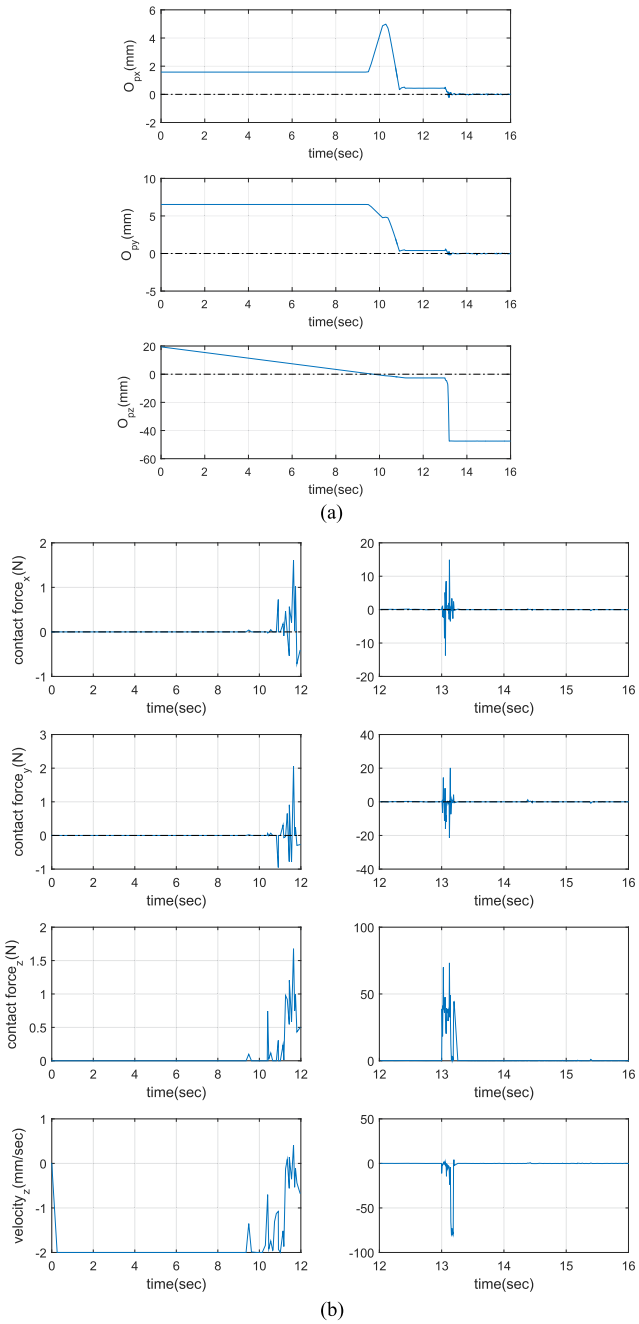

Fig. 8. (a) X-, Y-, and Z-component of the position of the center point of the lower surface of the crankshaft O_p. $t < 12$ s is the first phase. The crankshaft is pushed by a state-independent force to move along the boundary of the ARIE. When $t = 12$ s, the crankshaft is at the lowest point of the ARIE. $t \geq 12$ s is the second phase. As time passes, the uncertainty of the crankshaft is all eliminated and the insertion is achieved. (b) X-, Y-, and Z-component of the contact force between the crankshaft and the bearing, and the velocity of the crankshaft in the $O_h Z_h$ direction.

1) For the Crankshaft: The coordination frame for the crankshaft and the hole has been established in [24], as shown in Fig. 7(a), and the strategy has also been discussed. When the suitable θ_z is selected, the process reduces to a typical peg-hole insertion problem.

2) For the Input Shaft: The base coordinate frame $O_h X_h Y_h Z_h$ is fixed on the upper surface of the case. The base points of coordinates $O_{p'} X_{p'} Y_{p'} Z_{p'}$ and $O_p X_p Y_p Z_p$ are corresponding to the positions of upper and lower surface centers of the input shaft, respectively. The pose of the input shaft in

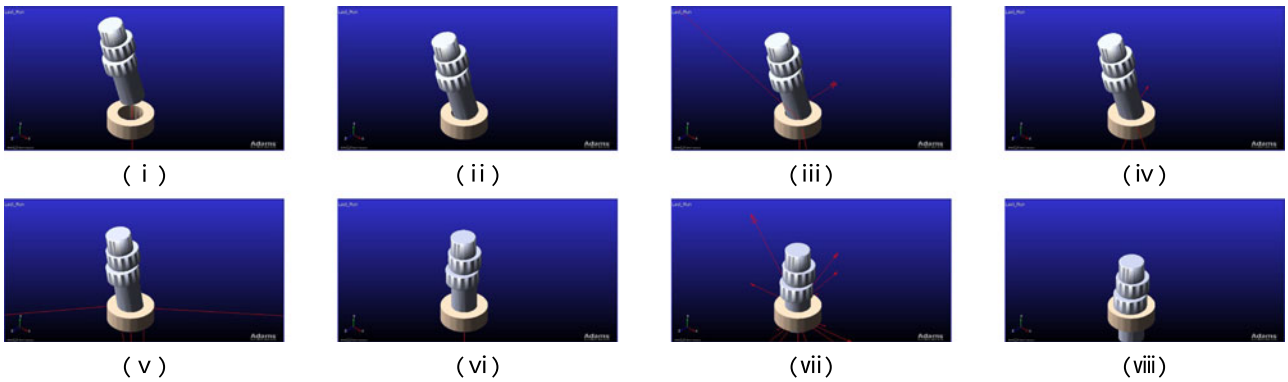

Fig. 9. Whole process of the simulation of crankshaft-bearing insertion where the initial position of O_p is $(5, -5, 10)$. (i)–(iv) First phase. The rotational angles of the crankshaft are fixed and a state-independent force is applied in the vertical direction, which pushes the crankshaft to the three-point contact state. (v)–(viii) Second phase. The crankshaft is gradually rotated along the Z_h-axis and the insertion is finally achieved.

$O_h X_h Y_h Z_h$ frame can be represented as

$$P_{\text{in}} = \left[|O_h O_p|_{X_h}, |O_h O_p|_{Y_h}, |O_h O_p|_{Z_h}, \theta_{X_h}, \theta_{Y_h}, \theta_{Z_h}\right]^T \triangleq [x, y, z, \theta_{X_h}, \theta_{Y_h}, f(\theta_z)]^T \in C_{\text{free}} \subset SE(3).$$

The input shaft is rotational symmetric about Z_p-axis. Therefore, the position of input shaft $[x, y, z]^T$ is not changed by θ_z and the constrained region formed by input shaft and the case is similar to a convex-peg-convex-hole ARIE.

As mentioned in Section IV-A, the assembly process of the parts can be divided into two phases. In each phase, the uncertainties will be eliminated within the pose of the shaft in different degrees of freedom (DoF). In this process, a state-independent force is applied along the Z_h-axis, and the state of the shaft will finally converge to the stable point.

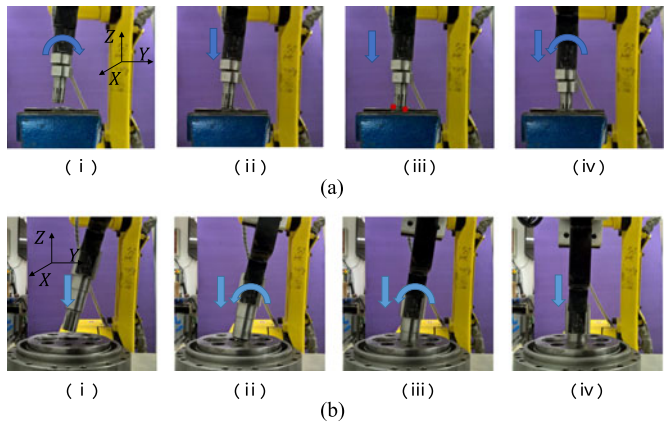

Fig. 10. Whole process of (a) crankshaft-bearing assembly and (b) input shaft case assembly.

B. Analysis of the Assembly Process Based on MSC.ADAMS

In this section, the crankshaft and bearing is taken as the example to illustrate how to achieve the insertion in ADAMS-based simulation environment. The main process of the assembly is made up of two phases. The position of the center point of the lower surface of the crankshaft is shown in Fig. 8(a) and the contact force between the crankshaft and the bearing is depicted in Fig. 8(b).

1) In the First Phase ($t < 12$ s): The crankshaft starts with a fixed orientation by θ_r (Note that θ_r is selected by experience. The smaller the θ_r is, the less time the process will spend; the larger the θ_r, the deeper the strict stable point will be in the constrained region, which guarantees the effectiveness. Usually $5^\circ \leq \theta_r \leq 10^\circ$.) across the $O_h X_h$-axis (or $O_h Y_h$-axis). And the crankshaft is pushed by the assigned state-independent force to the stable point of the ARIE. In this phase, the contact occurred at time $t = 9$ s, when the peg started touching the hole. After that, the peg will switch one-point contact to two-points contact, and finally three-points contact, which corresponds to the strict stable points in the $\mathbb{R}^3$ configuration space. In this phase, the contact force in all directions is very small since a low velocity $v_z = -2\,\text{mms}^{-1}$ is set.

2) In the Second Phase ($t > 12$ s): The crankshaft will be gradually rotated back, and then the rotational uncertainty will be eliminated.

In this phase, there is only one hopping point at $t = 13$ s. At that time, the uncertainty of the crankshaft is eliminated and the peg is pushed vertically into the bearing.

In the analysis above, it can be seen that there is a simple relation between the velocity of the assembly parts and the contact force. Therefore, in the real environment if there is requirement for less stress during the assembly process, the set value of the velocity should be set smaller to achieve the assembly.

Fig. 9 shows the process of crankshaft-bearing insertion in simulation environment for RV reducer assembly with different initial positions.

C. Experiment

To illustrate the effectiveness of the proposed strategy, two experiments are implemented with a Funuc M-6*i*B, which is a 6-axis industrial robot with repeatability of ± 0.08mm. The experimental setup is shown in Fig. 7(b) and (c). For the crankshaft-bearing insertion, the bearing is fixed on the workspace, and the

TABLE II
EXPERIMENTAL RESULTS OF RELIABILITY

No. of Exp.	Peg Diameter [mm]	Hole Diameter [mm]	Clearance [mm]	Strategy	No. of Trial	No. of Success	Success Ratio [%]
1.	9.75 (Crankshaft)	9.80 (Bearing)	0.05	Intuitive	50	31	62
				ARIE-based	50	50	100
2.	29.50, 26.50, 22.50 (Input shaft)	30.00 (Case)	0.50, 3.50, 7.50	Intuitive	50	40	80
				ARIE-based	50	49	98

crankshaft is placed in a set position. The 6-DoF robot with a 2-pin gripper will grab the crankshaft and then put it into the bearing. For the input shaft-case insertion, the case is fixed on the workspace, and the input shaft is placed in a set position. The 6-DoF robot with a 2-pin gripper will grab the input shaft and then put it into the case. The vision sensor is optional for locating the initial position of the crankshaft and the input shaft.

Combined with the strategy designed in configuration space, and the contact force analysis from the simulation stage, the assembly for crankshaft-bearing and input shaft case can be achieved.

It should be noted that to realize the proposed strategy, the robotic system should possess the following properties.

1) It should have some kind of "soft float" function, which means the manipulator could hold some freedoms of degree fixed during the movement.
2) It should have the ability to confine the maximum output force applied to the end effector so that it would not damage the assembly parts.

The whole process is shown in Fig. 10(a) and (b).

1) Assembly for Crankshaft and Bearing: The main difference between the simulation and the practical experiment is that the lower part of the crankshaft is gear-like. Since the contour of the side surface of the crankshaft is still cylindrical, it makes little difference in the real insertion process.

The steps for assembling the crankshaft are as follows.

1) The crankshaft is rotated across the x-axis by 10°.
2) The crankshaft is pushed by a state-independent force along the z-axis to the initial contact state.
3) Keep applying the force. The crankshaft is then pushed to the stable contact state.
4) The crankshaft is rotated back to achieve the insertion.

2) Assembly for Input Shaft and Case: The main difficulty for the insertion of input shaft is that the lower part is layered with regressive radius. Using backprojection, several ARIEs can be found in the different steps of the insertion process.

The steps for assembling the input shaft are as follows.

1) To insert the first layer to the case, the input shaft is rotated across the x-axis by 10°.
2) The input shaft is pushed by a z-axis state-independent force to the initial contact state. Keep applying the force. The input shaft is then pushed to the first stable contact state where the first layer is inserted.
3) Keep applying the force, hold the translational DoFs unfixed, and rotate the input shaft back to the second stable contact state.
4) Repeat the process to finish the insertion of the third layer.

To illustrate the reliability of the ARIE-based strategy, each experiment was conducted 50 times and compared with the intuitive strategy, which means that the peg would be pushed into the hole vertically. Through all experiments, the initial positional and rotational uncertainty was set randomly satisfying $|\Delta\theta| < 1.5°$ and $|\Delta x| < 0.50\,\text{mm}$. As shown in Table II, the intuitive strategy got only 62% success ratio for crankshaft-bearing insertion since the repeatability of the robot cannot meet the requirement of the clearance of the parts. With the initial uncertainty, jamming occurred inevitably during the insertion process. On the other hand, ARIE-based strategy achieved high reliability by means of the environment constraint and the properties of the robotic system.

VI. CONCLUSION

In this paper, the relation between the physical space and the configuration space for the robotic assembly system has been discussed. First, a series of theorems and proofs have been given to illustrate the general relation between the shape of the constrained region in configuration space and the geometry of the assembly parts in physical space. The existence of ARIE has been proven for convex-peg-convex-hole system, which can be used to achieve high-precision assembly. Second, the strategy investigation based on ARIE has been analyzed for round-peg-round-hole, and convex-polygon-peg-convex-polygon-hole insertion. A two-step strategy can be made to achieve the insertion. Third, an application of two types of peg-hole assembly for RV reducer with the concept of ARIE has been proposed. Based on the analysis and simulation, the experiments have verified the validity of the concept of ARIE and the ARIE-based strategy for part assembly.

In the future work, the concept is expected to be applied to more areas, such as service industry, where the ability to perform flexible manipulation is of great importance and is the basis to realize human–robot interaction with safety and reliability. In this work, ARIE focuses on the compliance formed by constraints of the environment. In the future work, ARIE-based method is expected to be integrated with coarse sensing information to increase the generality and robustness of the system, which could further helps to achieve low-cost and high-precision robotic systems.

REFERENCES

[1] R. Usubamatov and K. W. Leong, "Analyses of pegle jamming in automatic assembly machines," *Assem. Autom.*, vol. 31, no. 4, pp. 358–362, 2011.

[2] H. Bruyninckx, S. Dutre, and J. De Schutter, "Peg-on-hole: A model based solution to peg and hole alignment," in *Proc. IEEE Int. Conf. Robot. Autom.*, 1995, pp. 1919–1924.
[3] H. Qiao, C. Li, P. Yin, W. Wu, and Z. Y. Liu, "Human-inspired motion model of upper-limb with fast response and learning ability – A promising direction for robot system and control," *Assem. Autom.*, vol. 36, no. 1, pp. 97–107, 2016.
[4] R. Li, W. Wu, and H. Qiao, "The compliance of robotic hands–from functionality to mechanism," *Assem. Autom.*, vol. 35, no. 3, pp. 281–286, 2015.
[5] B. Shirinzadeh, Y. M. Zhong, P. D. W. Tilakaratna, Y. L. Tian, and M. M. Dalvand, "A hybrid contact state analysis methodology for robotic-based adjustment of cylindrical pair," *Int. J. Adv. Manuf. Technol.*, vol. 52, no. 1–4, pp. 329–342, 2011.
[6] Y. L. Kim, H. C. Song, and J. S. Song, "Hole detection algorithm for chamferless square pegin-hole based on shape recognition using f/t sensor," *Int. J. Precis. Eng. Manuf.*, vol. 15, no. 3, pp. 425–432, 2014.
[7] Z. Jakovljevic, P. B. Petrovic, V. D. Mikovic, and M. Pajic, "Fuzzy inference mechanism for recognition of contact states in intelligent robotic assembly," *J. Intell. Manuf.*, vol. 25, no. 3, pp. 571–587, 2014.
[8] S. R. Huang, K. Murakami, Y. Yamakawa, T. Senoo, and M. Ishikawa, "Fast peg-and-hole alignment using visual compliance," in *Proc. IEEE/RSJ Int. Conf. Intell. Robots Syst.*, Tokyo, Japan, Nov. 2013, pp. 286–292.
[9] S. R. Huang, Y. Yamakawa, T. Senoo, and M. Ishikawa, "Realizing peg-and-hole alignment with one eye-in-hand high-speed camera," in *Proc. IEEE/ASME Int. Conf. Adv. Intell. Mech.*, Tokyo, Japan, Jul. 2013, pp. 1127–1132.
[10] S. Huang, Y. Yamakawa, T. Senoo, and M. Ishikawa, "Dynamic compensation by fusing a high-speed actuator and high-speed visual feedback with its application to fast peg-and-hole alignment," *Adv. Robot.*, vol. 28, no. 9, pp. 613–624, 2014.
[11] R. J. Chang, C. Y. Lin, and P. S. Lin, "Visual-based automation of peg-in-hole microassembly process," *J. Manuf. Sci. Eng.*, vol. 133, no. 4, pp. 041015-1–041015-12, 2011.
[12] H.-Y. Jang, H. Moradi, S. Lee, and J. Han, "A visibility-based accessibility analysis of the grasp points for real-time manipulation," in *Proc. IEEE/RSJ Int. Conf. Intell. Robots Syst.*, Aug. 2005, pp. 3111–3116.
[13] B. Wang, L. Jiang, J. W. Li, and H. G. Cai, "Grasping unknown objects based on 3d model reconstruction," in *Proc. IEEE/ASME Int. Conf. Adv. Intell. Mech.*, 2005, pp. 461–466.
[14] S. Simunovic, "Force information in assembly processes," in *Proc. 5th Int. Symp. Ind. Robots*, 1975, pp. 415–431.
[15] D. E. Whitney and J. M. Rourke, "Mechanical behavior and design equations for elastomer shear pad remote center compliances," *J. Dyn. Syst. Meas. Control*, vol. 108, no. 3, pp. 223–232, 1986.
[16] R. K. Jain, S. Majumder, and A. Dutta, "Scara based peg-in-hole assembly using compliant ipmc micro gripper," *Robot. Auton. Syst.*, vol. 61, no. 3, pp. 297–311, 2013.
[17] R. K. Jain, S. Datta, S. Majumder, and A. Dutta, "Development of multi micro manipulation system using IPMC micro grippers," *J. Intell. Robot. Syst.*, vol. 74, no. 3/4, pp. 547–569, 2014.
[18] B. Baksys, S. Kilikevicius, and A. Chadarovicius, "Experimental investigation of vibratory assembly with passive compliance," *Mechanika*, vol. 17, no. 6, pp. 608–614, 2011.
[19] S. Kilikevicius and B. Baksys, "Dynamic analysis of vibratory insertion process," *Assem. Autom.*, vol. 31, no. 3, pp. 275–283, 2011.
[20] E. Sadauskas and B. Baksys, "Alignment of the parts using high frequency vibrations," *Mechanika*, vol. 19, no. 2, pp. 184–190, 2013.
[21] E. Sadauskas, B. Baksys, and V. Jurenas, "Elastic vibrations of the peg during part alignment," *Mechanika*, vol. 19, no. 6, pp. 676–680, 2013.
[22] C. Natale, R. Koeppe, and G. Hirzinger, "A systematic design procedure of force controllers for industrial robots," *IEEE/ASME Trans. Mechatronics*, vol. 5, no. 2, pp. 122–131, Jun. 2000.
[23] H. P. Chen, J. J. Wang, G. Zhang, T. Fuhlbrigge, and S. Kock, "High-precision assembly automation based on robot compliance," *Int. J. Adv. Manuf. Technol.*, vol. 45, no. 9, pp. 999–1006, 2009.
[24] S. J. Kwak, T. Hasegawa, and S. Y. Chung, "A framework for automatic generation of a contact state graph for robotic assembly," *Adv. Robot.*, vol. 25, no. 13/14, pp. 1603–1625, 2011.
[25] J. Takahashi, T. Fukukawa, and T. Fukuda, "Passive alignment principle for robotic assembly between a ring and a shaft with extremely narrow clearance," *IEEE/ASME Trans. Mechatronics*, vol. 21, no. 1, pp. 196–204, Feb. 2016.
[26] H. Qiao, M. Wang, J. Su, S. Jia, and R. Li, "The concept of 'attractive region in environment' and its application in high-precision tasks with low-precision systems," *IEEE/ASME Trans. Mechatronics*, vol. 20, no. 5, pp. 2311–2327, Oct. 2015.
[27] J. H. Su, H. Qiao, Z. C. Ou, and Y. R. Zhang, "Sensorless insertion strategy for an eccentric peg in a hole of the crankshaft and bearing assembly," *Assem. Autom.*, vol. 32, no. 1, pp. 86–99, 2012.

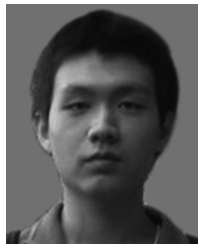

Rui Li received the B.Eng. degree in automation engineering from the University of Electronic Science and Technology of China, Chengdu, China, in 2013. He is currently working toward the Ph.D. degree with the Institute of Automation, Chinese Academy of Science, Beijing, China.

He is currently a Research Assistant with the Institute of Automation, Chinese Academy of Science. His current research interests include robotic compliance, intelligent robot system, and high-precision robotic manipulation.

Hong Qiao (SM'06) received the B.Eng. degree in hydraulics and control, and the M.Eng. degree in robotics from Xi'an Jiaotong University, Xian, China, in 1986 and 1989, respectively; the M.Phil. degree in robotics and control from the University of Strathclyde, Strathclyde, U.K., in 1997; and the Ph.D. degree in robotics and artificial intelligence from De Montfort University, Leicester, U.K., in 1995.

She held teaching and research positions at universities in the U.K. and Hong Kong from 1990 to 2004. She is currently a 100-Talents Project Professor with the State Key Laboratory of Management and Control for Complex Systems, Institute of Automation, Chinese Academy of Sciences, Beijing, China. She is the first to propose the concept of the attractive region in environment in strategy investigation, which was later successfully applied for robot assembly, robot grasping, and part recognition, which is reported in *Advanced Manufacturing Alert* (Wiley, 1999). Her current research interests include robotic manipulation, robotic vision, bioinspired intelligent robot, brain-like intelligence, etc.

Dr. Qiao is a member of the Administrative Committee of the IEEE Robotics and Automation Society (2014–2016, 2017–2019), the IEEE Medal for Environmental and Safety Technologies Committee (2014–2018), and the Robotics and Automation Society Long Range Planning Committee (2016–2017). She is on the editorial boards of five IEEE TRANSACTIONS and is the Editor-in-Chief of *Assembly Automation*.